Magnetized Disruption of Inertially Confined Plasma Flows

M. J.-E. Manuel,[1] A. B. Sefkow,[2,3,4] C. C. Kuranz,[5] A. M. Rasmus,[5,*] S. R. Klein,[5] M. J. MacDonald,[5,†]
M. R. Trantham,[5] J. R. Fein,[7,‡] P. X. Belancourt,[5] R. P. Young,[5] P. A. Keiter,[5] B. B. Pollock,[6] J. Park,[4,§]
A. U. Hazi,[6] G. J. Williams,[6] H. Chen,[6] and R. P. Drake[5]

[1]*General Atomics, Inertial Fusion Technologies, San Diego, California 92121, USA*
[2]*Department of Mechanical Engineering, University of Rochester, Rochester, NY 14623, USA*
[3]*Department of Physics and Astronomy, University of Rochester, Rochester, NY 14623, USA*
[4]*Laboratory for Laser Energetics, University of Rochester, Rochester, NY 14623, USA*
[5]*Department of Climate and Space Science and Engineering, University of Michigan, Ann Arbor, Michigan 48109, USA*
[6]*Lawrence Livermore National Laboratories, Livermore, California 94550, USA*
[7]*Department of Nuclear Engineering and Radiation Science, University of Michigan, Ann Arbor, MI 48109, USA*

The creation and disruption of inertially collimated plasma flows are investigated through experiment, simulation, and analytical modeling. Supersonic plasma jets are generated by laser-irradiated plastic cones and characterized by optical interferometry measurements. Targets are magnetized with a tunable B field with strengths of up to 5 T directed along the axis of jet propagation. These experiments demonstrate a hitherto unobserved phenomenon in the laboratory, the magnetic disruption of inertially confined plasma jets. This occurs due to flux compression on axis during jet formation and can be described using a Lagrangian-cylinder model of plasma evolution implementing finite resistivity. The basic physical mechanisms driving the dynamics of these systems are described by this model and then compared with two-dimensional radiation-magnetohydrodynamic simulations. Experimental, computational, and analytical results discussed herein suggest that contemporary models underestimate the electrical conductivity necessary to drive the amount of flux compression needed to explain observations of jet disruption.

The dynamics and evolution of collimated plasma flows are important to many physical systems, including shaped charges (SCs) [1], in inertial fusion [2] at the hohlraum wall [3] and inside the implosion during deceleration [4], and in a variety of astrophysical objects including young stellar objects [5,6], active galactic nuclei [7], and protoplanetary nebulae [8]. In terrestrial systems, these flows are generated and sustained predominantly through hydrodynamic processes. If magnetic fields are present in these systems, they exist in a regime where the ratio of hydrodynamic- to magnetic pressures (β) is quite high ($\gtrsim 10^4$); the detailed effects of externally applied or self-generated B fields in these systems is an area of intense investigation [1,3,9]. Work described in this Letter demonstrates a hitherto unobserved phenomenon, the magnetic disruption of inertially confined plasma jets in an as yet untested regime.

Experiments executed at the Jupiter Laser Facility utilized laser-irradiated plastic cones to produce inertially collimated, supersonic plasma flows through purely hydrodynamic processes [10]. A schematic of the target is shown in Fig. 1(a). The apex of the cone is irradiated with a $\sim$10-ns-square pulse containing $\sim$300 J ($\pm$15%) and shaped by phase plates to create a super Gaussian profile ($n \sim 2.5$) with a $\sim$750 μm diameter. Laser-driven shocks propagate through the cone and create a radially converging

plasma on the backside that accumulates on axis to produce an inertially confined jet, similar to the astrophysical formation process described by Canto *et al.* [5], though with additional axial flow. A solenoid [10,11] magnetizes the targets with a B field aligned along the jet propagation direction prior to laser irradiation, as schematically shown in Fig. 1(b). B-field effects on jet morphology are characterized by imaging interferometry using an optical probe beam.

The free-electron density of the plasma is inferred from two-dimensional (2D) interferograms. A sample raw data image is shown in Fig. 2(a) where the perturbed fringes
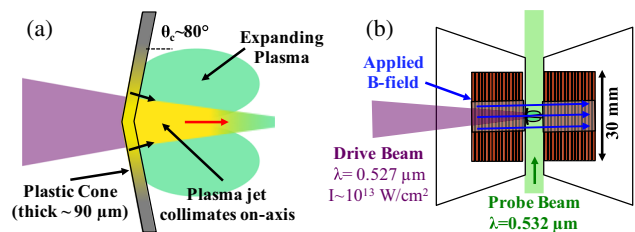

FIG. 1. (a) The schematic illustrates the formation of an inertially collimated jet created by laser irradiation of the cone apex. (b) Targets are magnetized prior to laser irradiation by a solenoid that applies a B field along the primary flow direction.
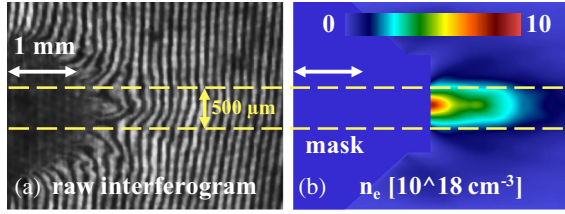
FIG. 2. A raw interferogram taken at 50 ns is presented in (a) with the inferred electron-density map shown in (b). A mask is used for areas where the phase change information is compromised.

indicate a local phase shift of the probe beam. The magnitude of this shift is linearly proportional to the path-integrated free-electron density for $n_e \ll n_{cr} \sim 4 \times 10^{21}$ cm^{-3}, where n_{cr} is the critical density for the probe's wavelength. For the low temperatures (simulated [10] $T_e \lesssim 1$ eV) of these break-out plasmas, bound electrons can also affect the phase shift of the probe in a nontrivial manner [10,12]. To minimize these effects, our analysis is restricted to the low-density regions of the plasma jet of interest, as shown in Fig. 2(b).

Phase-shift maps are unfolded from 2D interferograms using the wavelet analysis in Neutrino [13]. By assuming cylindrical symmetry, an Abel-inversion algorithm processes the top and bottom halves of the image which are averaged together to create the symmetric image shown in Fig. 2(b). This methodology allows us to determine a systematic, pixel-by-pixel uncertainty in the inferred electron density distribution that accounts for the symmetric assumption. The typical variation of the inferred electron density is $\lesssim 30\%$ for $r \gtrsim 75$ μm. Because of the high numerical error caused by the inversion process at small r, a smoothing function is implemented for $r \lesssim 75$ μm to ensure a zero derivative at $r = 0$.

Experiments performed with an imposed axial B field demonstrate the disruption of the inertial-confinement process due to increased field strength, as shown in
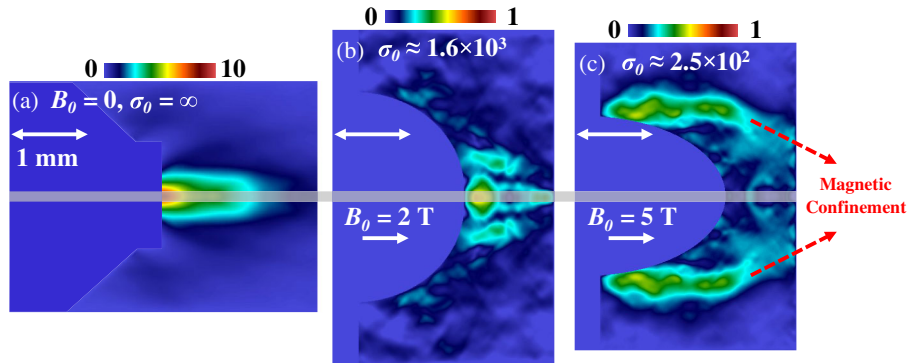
Fig. 3. Application of a 2-T B field is shown to partially inhibit the confinement since at $\sim$50 ns there is still some denser material on axis, though it is more inhomogeneous than in the no-field case. Increasing the background field strength by a factor of 2.5 produces vastly different plasma behavior. A B field of 5 T completely disrupts the inertial-confinement process, while also magnetically confining the expanding plasma. This envelope structure and magnetic focusing have been observed in previous simulations [14] and experiments [15] of laser-driven flat foils with the magnetic field aligned with the expanding flow. This phenomenon is observed here at large radii in conjunction with the disruption of the inertially collimated jet on axis.

The presence of the axial B field disrupts the inertial collimation process through its amplification and the resulting increase in magnetic pressure. The collimation process observed in cylindrical geometry may be described by a reduced, Lagrangian-cylinder (LC) model [1] that allows for a finite resistivity of the high-density, partially ionized system. In this description, a uniform cylindrical volume of initial radius R_0 and length L_0 has a constant axial velocity v_{z0} with an initially uniform, embedded B-field B_{z0}. For ease of notation, we introduce the elongation factor $n = L(t)/L_0$, where $L(t) = L_0 + v_{z0}t$ due to the approximately constant axial velocity. The radius of the cylinder R can then be written $R = R_0/\sqrt{n}$. As the cylinder propagates during the inertial collimation process, the radius shrinks ($dR/dt < 0$) and the length increases. The Ohm's Law for this system is written as $\mathbf{E} = \eta\mathbf{j} - \mathbf{v} \times \mathbf{B}$, where η is the plasma resistivity. Using this model, the B field along the axis $B_c(t)$ can be described [1] by

$$B_z(r = 0, t) = B_c(t) = B_{z0}ne^{-\frac{(n^2-1)}{2\mathrm{Re}_m}}, \qquad (1)$$

where $\mathrm{Re}_m = \mu_0 v_{z0} R_0^2/(4L_0\eta)$ is the magnetic Reynolds number, the ratio of B-field advection to diffusion. We note

FIG. 3. Inferred electron-density distributions from interferograms taken at $\sim$50 ns for (a) $B = 0$ T, (b) $B = 2$ T, and (c) $B = 5$ T. A background axial B field is shown to disrupt the formation of the jet on axis. These effects may be characterized by the inertial strength of the system, $\sigma_0 = \rho v_{z0}^2/p_{B0}$, where p_{B0} is the initial magnetic pressure. The gray centerline shows the extent of the smoothing function.
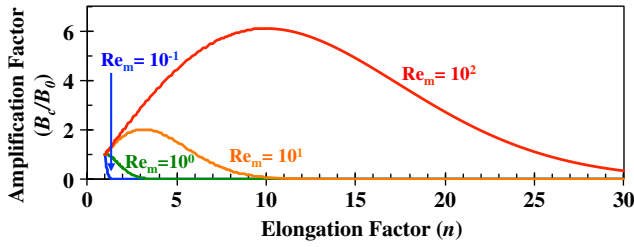
FIG. 4. Equation (1) is normalized and plotted against the elongation factor n. The amplification factor of the axial B field evolves due to the competing advection and diffusion processes occurring within the converging cylinder.

FIG. 5. The collimation parameter (ψ) is plotted for multiple σ_0 values at $\text{Re}_m = $ (a) 1, (b) 30, and (c) 100 where the shaded regions ($\psi > 0$) represent a parameter space that supports inertial collimation. In these calculations, $\beta_0 = 1$ defines an upper estimate for the initial plasma pressure, $R_0 = 375\ \mu$m is the approximate laser spot size, and $L_0 = 90\ \mu$m is the initial cone thickness.

here that the elongation factor n is a convenient measure of time and is used in the following discussion.

Equation (1) describes the evolution of the axial B field under conditions with a specified Re_m. This equation indicates that if diffusion of field lines through the plasma is important (i.e., $\text{Re}_m \lesssim 1$), then the axial field diffuses out as the cylinder elongates. However, if field advection is dominant ($\text{Re}_m \gg 1$), then the axial B field will be amplified in time, as illustrated in Fig. 4. For $\text{Re}_m > 1$, the field is amplified by a factor greater than one with a maximum reached at an elongation factor of $n_{\max} = \sqrt{\text{Re}_m}$, after which point diffusion across the converging cylinder begins to take effect as the radius shrinks. In this model, if $\text{Re}_m \leq 1$, any elongation at all reduces the axial B field.

To address the formation and disruption of a collimating jet in this model, we examine the radial pressure balance of our converging Lagrangian cylinder [1]

$$\rho \frac{dv_r}{dt} = -\frac{\partial p}{\partial r} + j_\phi B_z, \qquad (2)$$

where the azimuthal current (j_ϕ) is driven by the change in magnetic flux. In the following, we neglect the spatial dependence because the physics occurring near the axis determines the collimation of the jet. The pressure near the central axis $p_c(t)$ [i.e., $(r/R)^2 \ll 1$] may be expressed as

$$p_c(t) = \frac{1}{4}\frac{\rho v_{z0}^2}{n^3}\left(\frac{R_0}{L_0}\right)^2 - \frac{p_{th,0}}{\sqrt{n}} - \frac{B_{z0}^2}{2\mu_0}n^2 e^{-\frac{n^2-1}{\text{Re}_m}}, \qquad (3)$$

where the boundary condition $p(R)$ is set to the initial thermal pressure of the plasma ($p_{th,0}$) and reduces as $\sqrt{n}$ due to the increase in radial surface area caused by elongation. Negative terms represent pressures that expand the plasma radially, whereas positive terms indicate radial convergence. The first term in Eq. (3) is associated with the inertial collimation process that is initiated by the expansion of the cone-shaped target. The last two terms in Eq. (3) are the thermal and magnetic pressures, respectively, that act against the collimation process by causing the plasma to expand. By normalizing to the initial background magnetic pressure $p_{B0} = B_{z0}^2/(2\mu_0)$, the system is described by
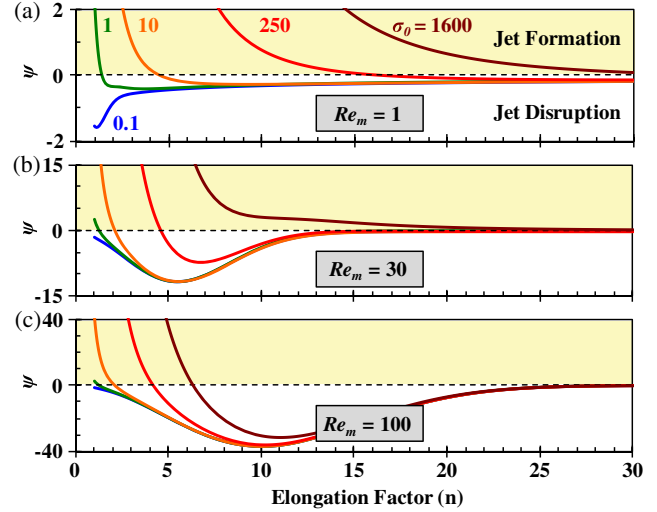
where the collimation parameter $\psi(= p_c/p_{B0})$ is a dimensionless parameter that determines whether the plasma is in a regime where inertial collimation may still form a jet in the presence of an axial B field. The collimation process is characterized by the inertial strength, $\sigma_0 = \rho v_{z0}^2/p_{B0}$, the plasma beta, $\beta_0 = p_{th,0}/p_{B0}$, and the magnetic Reynolds number Re_m. When $\psi > 0$, inertia (σ_0) dominates Eq. (4) and the conditions are favorable for collimation. Radial expansion driven by the thermal and magnetic pressures works against inertial collimation, reaching marginal stability when $\psi = 0$. Therefore, ψ may change sign, such that a well-collimated jet may be eventually disrupted by the amplification of an axial field, depending on the specific parameters of the flow. When $\psi < 0$, B-field amplification due to the converging flow is too great to allow a jet to form.

Figure 5 illustrates this complex space in the form of three plots of differing $_m$, wherein each plot contains the evolution of ψ for multiple values of σ_0. From these plots and the measurement-based values of σ_0 from Fig. 3, the qualitative behavior observed at 50 ns ($n \sim 28$) of total disruption with 5T and partial disruption with 2T is consistent with the LC model of a plasma with $\text{Re}_m \sim 1$–30. This is evident due to the fact that the $\sigma_0 = 1600$ (2T) case stays positive, but approaches zero up to $n = 30$, and the $\sigma_0 = 250$ (5T) case crosses zero before $n \sim 28$, consistent with observations. Additionally, using the typical values [16] of the plasma at this late stage of evolution, $\text{Re}_m \lesssim 30$ is calculated and is

$$\psi = \frac{1}{4}\left(\frac{R_0}{L_0}\right)^2 \frac{\sigma_0}{n^3} - \frac{\beta_0}{\sqrt{n}} - n^2 e^{-\frac{n^2-1}{\text{Re}_m}}, \qquad (4)$$
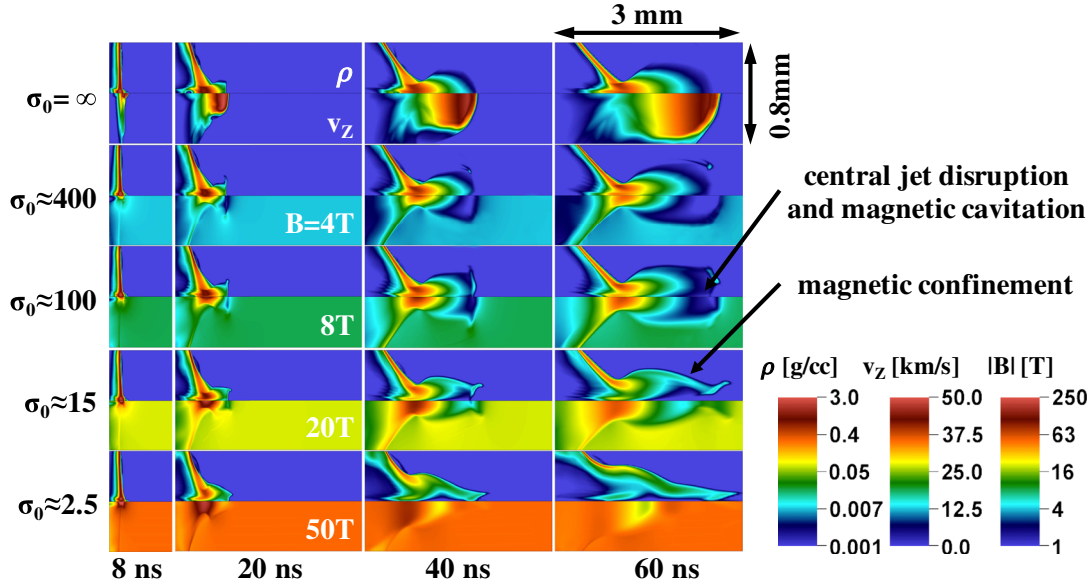
FIG. 6.   Simulation results from HYDRA with initial axial B fields of 0, 4, 8, 20, and 50 T. The top panel illustrates jet evolution for the nominal $B = 0$ case with density contours and axial velocity contours shown, spatially and temporally consistent with inertial collimation observed in the experiments; note the $2:1$ aspect ratio used to illustrate the jet morphology. Subsequent panels show jet evolution (density on top, B-field strength on the bottom) at increasing seed B-field strength. The level of inertial collimation is reduced as B increases, while the radially expanding plasma is more strongly magnetically collimated.

consistent with the ideal LC model. However, the experimental system is not homogenous or ideal, as the LC model assumes, and observations are made late in time due to the optical diagnostics implemented, even though, as the data and the model suggest, the disruption of the jet occurs earlier in its evolution.

To further investigate the disruption physics, a comprehensive set of radiation-magnetohydrodynamic simulations of a scaled system [18] were performed using the HYDRA [19,20] code. Figure 6 graphically summarizes the findings of this computational study where the applied B field was increased over a range from 0T in the top panel to 50T in the bottom panel. The baseline case (top panel in Fig. 6) shows that the scaled system evolves similarly to experiments in that a collimated jet is formed due to its own inertia, has a radius of ~400–500 μm and a length of ~2.5 mm at ~40–60 ns, and with a nominal axial velocity of ~50 km/s. Using this benchmarked model of the experiment, the imposed B field was included and its strength systematically increased to study the competing effects of inertial collimation, magnetic disruption of the central jet, and the magnetic collimation of the outwardly expanding plasma.

The bottom four panels of Fig. 6 show the effects of increasing the applied B-field strength on the collimated jet. At early times (<20 ns), the density distributions do not change much between the four cases, and all illustrate B-field amplification, as shown by the enhanced B-field strength on axis by 20 ns. It is this amplification which is necessary at smaller B fields (4T and 8T) for disruption to occur later in time, whereas at higher field strengths (20 and 50T) a mass deficit is observed on axis (i.e., no inertial

collimation) by 20 ns and magnetic collimation of the expanding plasma has begun. In the 8T case, the axial mass deficit begins at ~40 ns and is fairly well developed by the 60 ns panel where the central jet disruption is clearly visible. In the 20 and 50T cases, the inertially collimated jet never forms and the late-time panels simply show advanced development of the magnetically collimated, expanding plasma [14,15]. HYDRA calculations exhibit the expected behavior suggested by the LC model and motivated by experiments. However, to be consistent with experimental observations, the electrical resistivity was artificially reduced in order to provide enough flux compression early in the evolution to disrupt collimation at high inertial strengths ($\sigma_0 > 100$).

B-field amplification is possible when there is low-enough diffusion on the spatial and temporal scales over which flux compression occurs, i.e., when $Re_m > 1$. The amplification factor depends on Re_m, and increases as $\sqrt{Re_m}$ in the simple LC model. This suggests that a factor of 10 difference in calculated resistivity, for a simple model, can change the amplification factor by more than 3, which may result in a very different plasma evolution. When amplification begins, the collimating plasma is solid density (~1 g/cc) with a simulated (LEOS table 5070) temperature and ionization state of $\lesssim 1$ eV and ~1, respectively. Under these conditions, the implemented Lee-More [21] resistivity model (LM) gives values of order ~10^{-4} Ω cm; typical room-temperature conductors (e.g., copper) have resistivities of order ~10^{-6} Ω cm. Simulations using LM resistivity show no measurable effect on the plasma evolution at relevant seed B-field strengths, whereas

experimental observations clearly demonstrate a dramatic change in plasma behavior. Because ionization state and conductivity models in the $\sim$eV, $\sim$Mbar plasma regimes are not well tested, and the evolution depends greatly on the amplification process, this is the most likely source of error in the modeling. This error is mitigated by using a 10^{-2} multiplier on the resistivity, i.e., forcing the collimating plasma to be a typical room-temperature conductor, such that HYDRA calculations produce similar results to experiments at relevant B-field strengths. Alteration of LM transport coefficients by this magnitude in low-temperature, high-density plasmas is supported by density functional theory calculations that predict this behavior in plastic [22,23] and water [24].

In summary, our experimental results unequivocally demonstrate the disruption of an inertially collimated jet caused by a background axial B field. These are the first observations of such a disruption mechanism in this plasma regime with applications to research in shaped charges, inertial fusion energy, and astrophysics. The primary effects caused by the background field are captured by a Lagrangian-cylinder model that accounts for B-field advection and diffusion in radially converging systems. The model is parametrized by the magnetic Reynolds number (Re_m) and inertial strength (σ_0) of the system and suggests that the disruption physics occurs early in the jet evolution. Comprehensive 2D-radiation-hydrodynamic simulations explored the disruption physics in a more complete manner than the LC model by looking at the B-field amplification at early times during inertial collimation. These calculations indicate that the Lee-More resistivity model is insufficient in the regime of interest to explain the experimental results and that the eV, Mbar plasmas must have a lower resistivity than expected. The combination of experimental, analytical, and computational results discussed herein demonstrate that systems with high inertial strengths ($\sigma_0 \sim 10^2$–10^3), typical in laser-produced plasmas, can be strongly affected by B fields. This understanding opens a new methodology to test resistivity models in low-temperature, high-density plasmas.

*Present address: Los Alamos National Laboratories, Los Alamos, NM, USA.

†Present address: Lawrence Livermore National Laboratories, Livermore, CA, USA.

‡Present address: Sandia National Laboratories, Albuquerque, NM, USA.

§Present address: University of California, San Diego.

[1] S. V. Fedorov, Combust. Explos. Shock Waves, **41**, 106 (2005).

[2] J. D. Lindl, B. A. Hammel, B. G. Logan, D. D. Meyerhofer, S. A. Payne, and J. D. Sethian, Plasma Phys. Controlled Fusion, **45**, A217 (2003).

[3] C. K. Li et al., Phys. Rev. Lett. **102**, 205001 (2009).

[4] C. R. Weber et al., Phys. Plasmas, **22**, 032702 (2015).

[5] J. Cantó et al., Astron. Astrophys. **192**, 287 (1988).

[6] C. Carrasco-González, L. F. Rodriguez, G. Anglada, J. Marti, J. M. Torrelles, and M. Osorio, Science **330**, 1209 (2010).

[7] A. P. Marscher et al., Nature (London) **452**, 966 (2008).

[8] B. Balick, and A. Frank, Annu. Rev. Astron. Astrophys. **40**, 439 (2002).

[9] W. Fox, F. Sciortino, A. v. Stechow, J. Jara-Almonte, J. Yoo, H. Ji, and M. Yamada, Phys. Rev. Lett. **118**, 125002 (2017).

[10] M. J. E. Manuel et al., High Energy Density Phys., **17**, 52 (2015).

[11] S. R. Klein, M. J.-E. Manuel, B. B. Pollock, R. S. Gillespie, M. Deininger, C. C. Kuranz, P. A. Keiter, and R. P. Drake, Rev. Sci. Instrum. **85**, 11E812 (2014).

[12] E. C. Merritt, A. L. Moser, S. C. Hsu, C. S. Adams, J. P. Dunn, A. M. Holgado, and M. A. Gilmore, Phys. Plasmas **21**, 055703 (2014).

[13] A. Flacco et al., Neutrino v941+. Laboratoire d'Utilisation des Lasers Intenses, current version here, 2013.

[14] A. Ciardi, T. Vinci, J. Fuchs, B. Albertazzi, C. Riconda, H. Pépin, and O. Portugall, Phys. Rev. Lett. **110**, 025002 (2013).

[15] B. Albertazzi et al., Science **346**, 325 (2014).

[16] Late-time measurement of $n_e \sim 10^{18}$ cm^{-3}, simulated $T_e \sim 1$ eV, FLYCHK [17] local thermal equilibrium estimate of $\bar{Z} \sim 0.01$.

[17] H. K. Chung, W. L. Morgan, and R. W. Lee, J. Quant. Spectrosc. Radiat. Transfer **81**, 107 (2003).

[18] Cone half-angle is 60°, cone thickness is 30 μm, and laser energy is $\sim$100 J.

[19] M. M. Marinak, G. D. Kerbel, N. A. Gentile, O. Jones, D. Munro, S. Pollaine, T. R. Dittrich, and S. W. Haan, Phys. Plasmas **8**, 2275 (2001).

[20] A. B. Sefkow, S. A. Slutz, J. M. Koning, M. M. Marinak, K. J. Peterson, D. B. Sinars, and R. A. Vesey, Phys. Plasmas **21**, 072711 (2014).

[21] Y. T. Lee, and R. M. More, Phys. Fluids **27**, 1273 (1984).

[22] S. X. Hu et al., Phys. Plasmas **23**, 042704 (2016).

[23] D. Batani et al., Phys. Rev. E **61**, 5725 (2000).

[24] T. R. Mattsson, and M. P. Desjarlais, Phys. Rev. Lett. **97**, 017801 (2006).